NeatSkin: A Discrete Impedance Tomography Skin Sensor

Euan Judd, Krishna Manaswi Digumarti, Jonathan Rossiter, Helmut Hauser

***Abstract*— In this paper we present NeatSkin, a novel artificial skin sensor based on electrical impedance tomography. The key feature is a discrete network of fluidic channels which is used to infer the location of touch. Change in resistance of the conductive fluid within these channels during deformation is used to construct sensitivity maps. We present a method to simulate touch using this unique network-based, low output dimensionality approach. The efficacy is demonstrated by fabricating a NeatSkin sensor. This paves the way for the development of more complex channel networks and a higher resolution soft skin sensor with potential applications in soft robotics, wearable devices and safe human-robot interaction.**

I. INTRODUCTION

Soft robots are made of materials that are compliant when subjected to the range of forces expected under operation [1]. As such, they can demonstrate complex motions [2]–[4], requiring flexible and stretchable sensors for sensing a change in the body's state. A challenge of making sensors for soft robots is therefore to measure soft body dynamics and external stimuli without significantly increasing output dimensionality, reducing compliance and complex motion, which can be useful features [5], while the sensor also remains functional under large strains.

Sensorised skins have previously been proposed as a solution to sensing across the body surface [6]. Commonly used techniques involve the measurement of change in resistance, capacitance, magnetic flux and intensity of light [7], [8]. Sensors that rely on capacitance change [9]–[12] typically employ an orthogonal grid of electrodes separated by a layer of dielectric material. While they have been successful in detecting skin touch to a high resolution, the large number of electrodes required to cover the entire surface is a drawback. In contrast, our approach is based on electrical impedance tomography and employs a much smaller number of electrodes. Impedance tomography, thought to be first proposed in personal communication in the early 1970s by R. B. Pullan [13], involves non-invasive imaging of the internal structure of a body by measuring the electrical impedance between pairs of electrodes placed on its surface. This technique is commonly used in medical imaging and has been used in the design of artificial skins [14]–[17]. Those early designs use sheets of conductive fabrics and rubbers which can potentially reduce the compliance of the structure.

However, in this paper we propose a different approach. We use a network of channels filled with conductive fluid embedded within the skin to enable it to sense interactions

All authors are with Department of Engineering Mathematics, University of Bristol, BS8 1TH, United Kingdom, and with Bristol Robotics Laboratory, BS16 1QY, United Kingdom. (email: euan.judd@bristol.ac.uk)

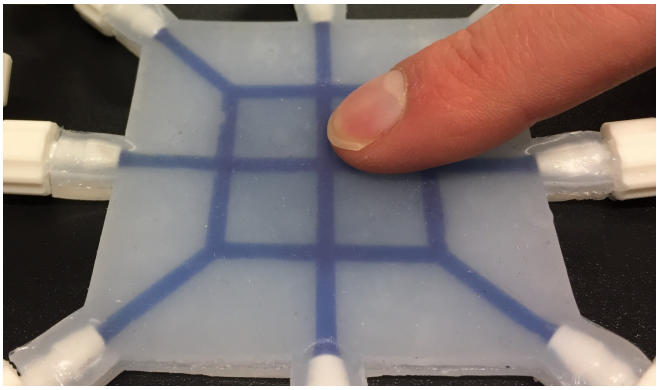

Fig. 1. A connected network of fluidic channels (blue dye added for clarity) fabricated in EcoFlex® 00-30 silicone.

(Fig. 1) similar to the network presented in [18] which used a network of ionic liquid. Opposed to [18], which used an inverse method for image reconstruction, we employed a machine learning approach to reduce output dimensionality and improve accuracy. By measuring changes in resistance caused by a change in the length and/or cross-sectional area of channels under structural deformation [19]–[21], information regarding the position of interaction can be inferred. Since a network of channels is used in the sensor as opposed to a continuous layer of fluid, there is opportunity to reduce the overall weight and increase the flexibility of the structure. Compared to other resistance based methods (e.g. [22]), the design presented here uses a single layer of sparse channels to determine the position of touch. We first present the results of a computer simulation of the proposed network approach. We then compare the simulation with experimental results before training a neural network to explore the performance of an artificial skin, NeatSkin, as a touch sensor.

II. SIMULATION

Conductive fluid in a channel can be described as a resistor using Pouillet's law

$$R = \rho L/A, \tag{1}$$

where ρ is the resistivity of the material, L is the length of the resistor and A is its cross-sectional area. In the case of the sensor, each section of the channel can be considered to be a resistor, the resistance of which changes through interaction with the environment.

In our skin, the channels were arranged in a grid-like configuration and electrodes were positioned at 8 different

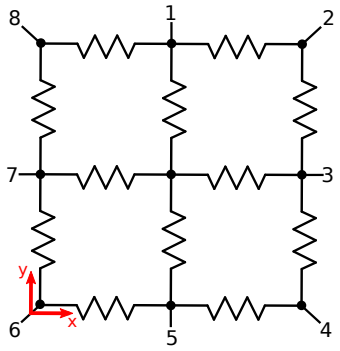

Fig. 2. In the theoretical model, the equivalent resistance was calculated between the 8 electrodes for a total of 28 electrode pair combinations. Each of the 12 channels was modelled as a single resistor with resistance, R, which was increased by 50% to simulate a touch.

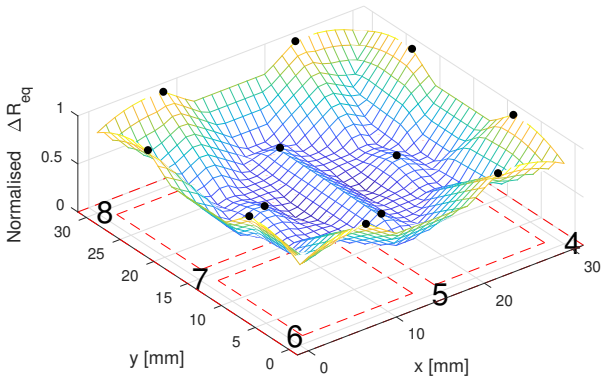

Fig. 3. The change in equivalent resistance (ΔR_{eq}) was found theoretically by increasing the resistance of the 12 resistors (black dots) by 50% one at a time. R_{eq} was calculated between all 28 electrode pairs, **S**, for each of the 12 resistance changes. The normalised [-1,1] maximum ΔR_{eq} for all **S** is plotted here. Dashed lines show the boundaries of the channel network. The theoretical results show a good sensitivity profile to resistance change although all resistance changes are simulating pressing directly on a channel and therefore sensitivity within the 4 quadrants between channels was not modelled.

locations to measure changes in resistance (Fig. 1). A simplified theoretical approximation is to model each channel as a resistor. (Fig. 2). The sensitivity of the network at a point (x, y) on the surface was defined as the maximum of the change in equivalent resistance between each pair of electrodes. This may be expressed as

$$z(x, y) = max(\Delta R_{eq}^{i,j}(x, y)), \tag{2}$$

where $\Delta R_{eq}^{i,j}(x, y)$ was the change in equivalent resistance measured between electrode pairs i and j ($i, j \in \{1, 2, \ldots 8\}$, $i \neq j$) when the resistance of a channel changes at location (x, y) and normalised to [-1,1] for comparison between simulated and experimental results. In our case, $\{x, y \in \mathbb{R} \,|\, 1mm \leq x, y \leq 30mm\}$.

To determine the sensitivity in simulation, the resistance of each channel was initially assumed to be equal and set to an arbitrarily chosen value R. The assumption of equality is valid since the length and cross-sectional area of all the channels is the same. The exact value of R is not relevant for comparison as ΔR_{eq} was normalised in both the simulation and experimental results.

To simulate a touch at the mid point of a channel, the resistance, R, of each resistor was increased by 50% and the equivalent resistance between each electrode pair was calculated using Python's Ahkab circuit simulator [23].

Measuring ΔR_{eq} between all combinations of 8 electrodes gives the set **S** of ${}^8C_2 = 28$ electrode pairs or signals, (e_i, e_j).

$$\mathbf{S} = \{(e_i, e_j) \,|\, i, j \in \{1, 2, \ldots, 8\}, i \neq j\} \tag{3}$$

Fig. 3 shows the maximum simulated sensitivity at each position for all pairs in **S** found using Eq. 2. Fig. 5(a)-(c), 5(g) and 5(h) shows the simulated sensitivity at each position for 5 of the 28 signals. All other electrode pairs in **S** are rotationally symmetric to one of these and are therefore not shown. Simulation results show that a change

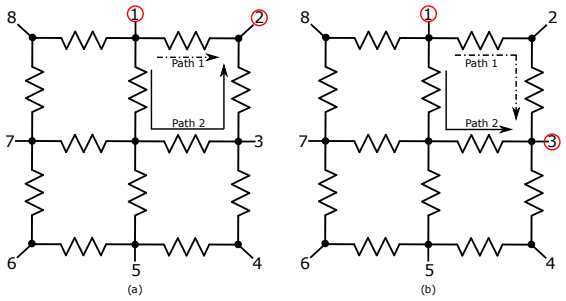

Fig. 4. (a) the ratio of the resistance along paths 1 and 2 between electrodes 1 and 2 is one third. (b) the ratio of resistance along paths 1 and 2 between electrodes 1 and 3 is one. The electrode pair (1,3) is therefore sensitive to a larger region of the sensor than pair (1,2).

in the resistance of any channel is detectable by one or more pairs in **S** as demonstrated by the nonzero sensitivity values along the channels (dashed lines) in Fig. 3. This analysis, though simplified, is useful for network design as it helps to understand the effect on sensitivity of a chosen network layout, the robustness of the network to a change in topology, and the number of electrodes needed and their positions on the sensor. For instance, adjacent electrode pairs have a high sensitivity to changes along the shortest path between them, but little sensitivity elsewhere (Fig. 5(a)). This is expected, as the path of least resistance is the shortest path due to the constant cross-sectional area and resistivity. Thus the difference in length between the two shortest paths, such as path 1 and path 2 between electrodes 1 and 2 in Fig. 4(a), result in high sensitivity along path 1 and little sensitivity elsewhere. This is also true for electrodes on

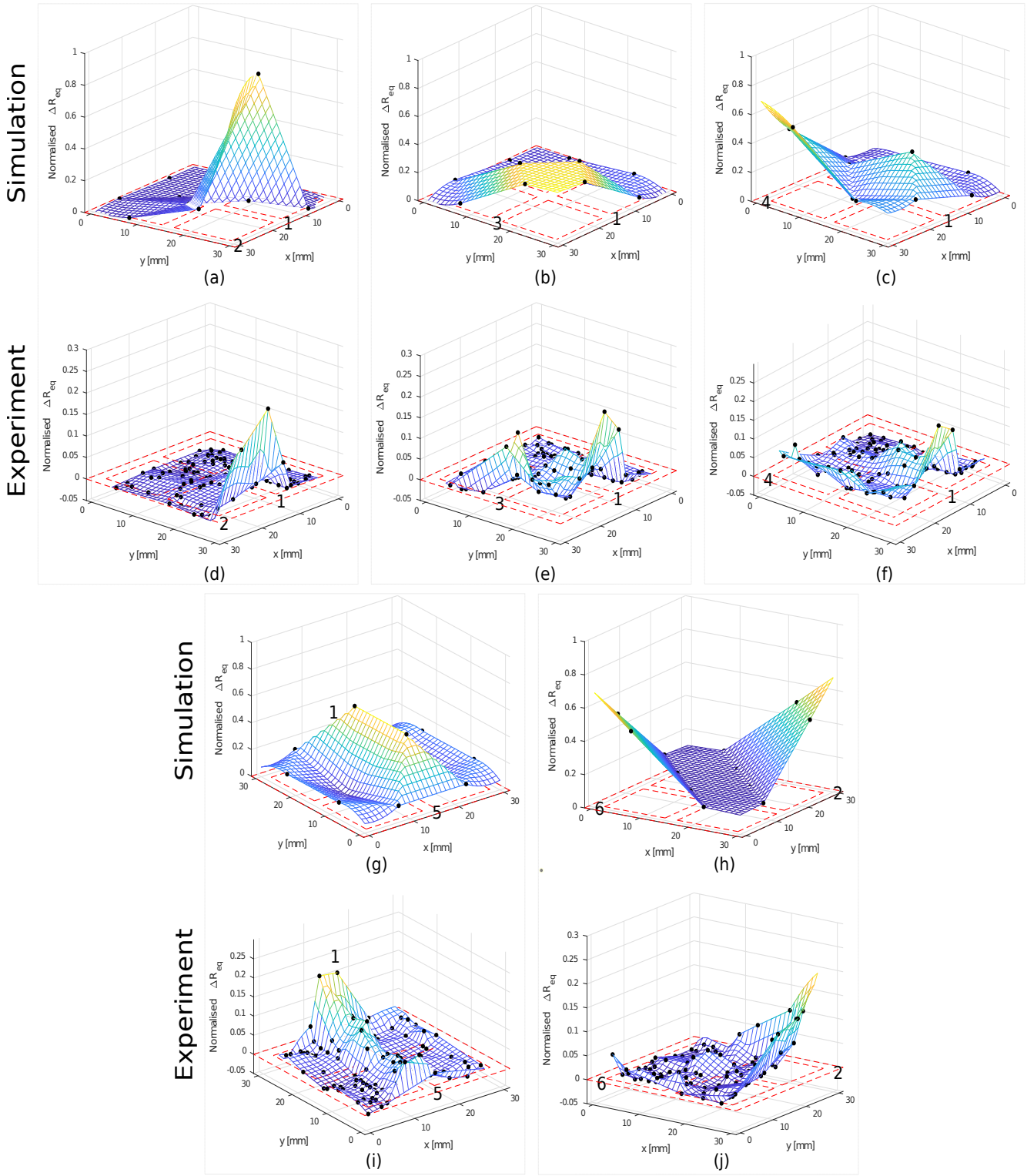

Fig. 5. The sensor has rotational symmetry when rotated by 90° about its centre. The change in equivalent resistance (ΔR_{eq}) is therefore unique for five electrode pairs and every other pair is a repetition of these five pairs. (a)-(c), (g), and (h) show the normalised [-1,1] theoretically calculated ΔR_{eq} while (d)-(f), (i), and (j) show the normalised [-1,1] experimentally obtained ΔR_{eq}. The dashed lines indicate the boundaries of the channels. Black dots in the figure are simulated/experimental locations of presses on the sensor. In theoretical work, ΔR_{eq} within the four quadrants appears to be high, such as the yellow patch in (b), however this is due to interpolation between the four surrounding test positions. This region in the experimental plot (e) shows a close to zero sensitivity in this region.

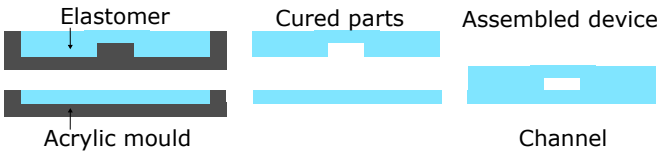

Fig. 6. An acrylic mould was used to cast EcoFlex® 00-30 silicone. The top layer was cast in a mould containing the channel network, also cut from acrylic, and the bottom layer was cast in the same mould without the channels. The two halves of silicone were then glued using silicone adhesive (SilPoxy, Smooth-On)

opposite edges of the sensor (electrode pair (1,5) in Fig. 5(g) and its rotationally symmetric pair (3,7)). If two or more paths between electrodes are of equal or almost equal length, then the electrode pair is sensitive to a larger area on the sensor. For instance, the length of path 1 in Fig. 4(b) is equal to the length of path 2. Two or more paths of equal length are also seen in electrode pairs (2,6), (1,3) and (1,4) (Fig. 5(h), 5(b) and 5(c) respectively), along with their rotationally symmetric pairs.

III. EXPERIMENTATION

A prototype NeatSkin sensor skin was fabricated (Fig. 1) to the network design in Fig. 2. A mould was fabricated using laser-cut acrylic sheets. The channel layout was glued to a flat sheet to make up one half of the mould. Silicone elastomer (EcoFlex® 00-30, Smooth-On) was cast in the mould and left to cure. The other half was a flat layer of silicone that was cast separately. The two cured parts were then glued together with silicone adhesive (SilPoxy, Smooth-On) to assemble the sensor (Fig. 6). The channels had a rectangular cross-section with a width of 2mm and a height of 1mm and the length of each channel section was 15mm. The total thickness of the sensor was 5.5mm.

Pneumatic fittings with a barbed end (Cole-Parmer) were inserted into the 8 network openings and glued in place. These fittings provided points of access to fill the network with fluid and allowed for removal of air bubbles within the network. 8 gold plated electrodes were then inserted into the fittings to electrically connect with the fluid channels.

The conductivity of tap water is a result of positive and negative ions of salt moving towards the cathode and anode respectively when a potential difference exists. The application of a DC voltage results in an accumulation of ions at the electrodes, thereby reducing conductivity over time. We therefore used a high frequency alternating current (AC) of 2mA at 1kHz [24]. In this case, the Lorentz force acting on the ions is continuously reversing, preventing the congregation of ions at the electrodes. This also minimises the problem of electrolysis of water that occurs at voltages above the electrolysis potential.

To account for the change in conductivity of water with temperature, and to remove bubbles, the network was flushed with new tap water before data acquisition. All experiments were conducted in a temperature controlled room at 22°C. All the data was collected on the same day.

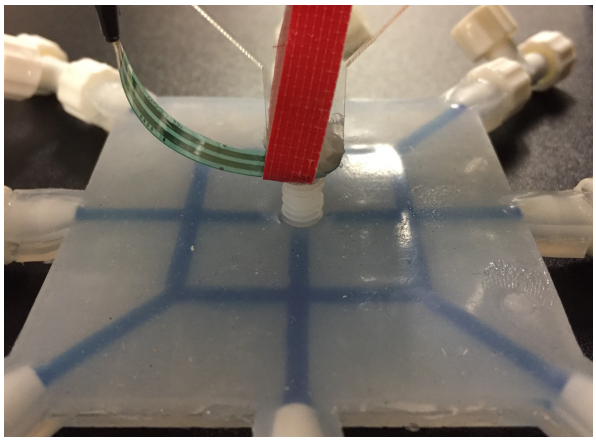

Fig. 7. A 3D printer was modified to use a probe to press different positions on the sensor. A force sensor was used to automatically label each position. 100 positions were pressed 28 times each while the change in voltage between each **S** was recorded.

Electrical measurements across **S**, the signals of the 28 electrode pairs, can then be used to predict each of the test positions. To perform the presses consistently and repeatably, a 3D printer was modified so that the extrusion nozzle was replaced by a probe (Fig. 7). The probe had a circular cross-section with a 5.5mm diameter and a flat surface that made contact with the sensor. This means that the distance between the nearest points on neighbouring channels of 13mm in the network is a little over 2 probe diameters (compare Fig. 7). The deformation of silicone when the probe is not pressed directly over a channel will still cause a reduction in the cross-sectional area of channels in its vicinity. A force sensor (Interlink Electronics FSR400 0.2" Diameter Force Sensing Resistor) was affixed between the probe and the print head to automate the detection of a press. On each press, the probe reached a depth of 3.5mm below the top surface of the sensor.

A total of 100 random positions for the presses were generated in G-Code and sent to the printer. These positions lie on the channels or within the central 4 quadrants of the sensor where quadrants are the square areas between the channels. A data acquisition device (NI USB-6229; National Instruments) was used to generate a sinusoidal zero-mean current wave and capture the resulting voltage change, measured with a laboratory galvanostat (HA-151B, Hokuto Denko), as well as the force sensor data with a 10kHz sampling rate. Signals for each pair in **S** were recorded in sequence. 7 analog multiplexers with 4 analog switches in each (MAX4052, Maxim) were used to cycle between the 28 pairs.

MATLAB was used to process the data. Moving root mean square (RMS) values of the current and voltage signals were calculated with a window of ten samples. Ohm's law was then used to calculate the resistance using these RMS values.

Sensitivity between electrode pairs for experimental data (Fig. 8 and Fig. 5(d)-(f), 5(i), 5(j)) mirrored theoretical results with a couple of key differences. The higher density of points for which ΔR_{eq} was measured show areas within

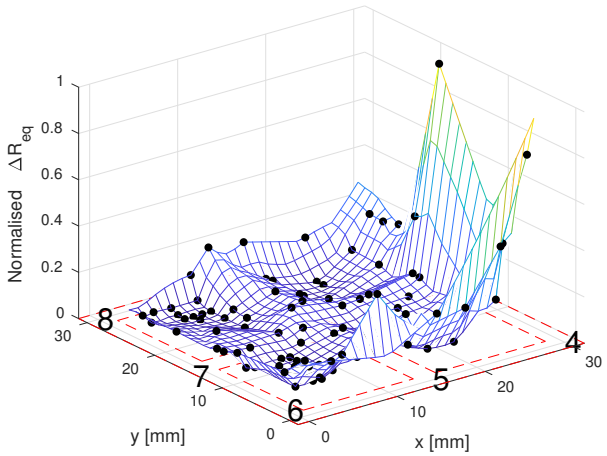

Fig. 8. Sensitivity of the fabricated sensor by plotting the changes in equivalent resistance (ΔR_{eq}) for each of the 100 data points measured for each **S**. The dashed lines indicate the boundaries of the channels. Results mirror theoretical calculations where the greatest sensitivity can be observed around the periphery. Pressing within the 4 quadrants shows good sensitivity when close to and on the channel network but low sensitivity for a small area within the centre of each quadrant.

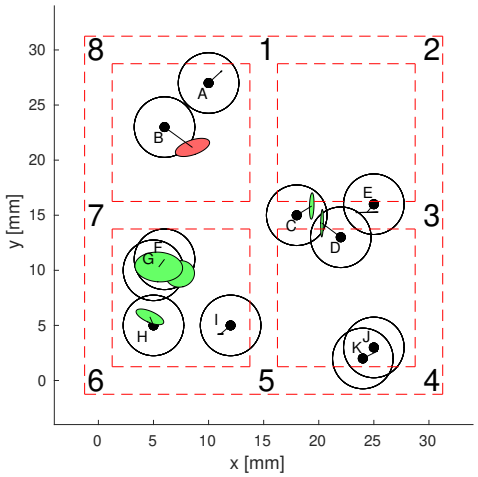

Fig. 9. The trained neural network model was used to predict the position of 11 randomly selected positions. The mean of 6 predictions per position and the standard deviation were plotted as green ellipses. The radius of the probes was 2.75mm and was plotted as a circle. The solid lines are between the centre of each circle and the centre of each ellipse where the latter is the mean prediction of the former. The mean prediction was within the probes radius for all but one position (B). The dashed lines indicate the boundaries of the channels.

the four quadrants where sensitivity was close to zero. This information was missing in the simulation. Results in Fig. 8 generally show higher ΔR_{eq} around the periphery except where it is relatively low (x = 0mm) and relatively high (x = 27mm). This is likely due to the alignment of the probe on the sensor during data acquisition. For instance, where ΔR_{eq} was relatively high, the likely cause was the channels leading to electrodes 3 and 4 being partially closed off. At the same time, where ΔR_{eq} was relatively low at the other side of the sensor, the probe was further from electrodes 7 and 8 and therefore did not close off the channels leading to these electrodes.

IV. PREDICTIONS

A feed-forward neural network with a single layer containing 5 neurons was implemented in MATLAB and used to predict the location of a press given measurement set **S**. One layer has been shown to approximate any continuous function to reasonable accuracy with less risk of over-training [25]. The Levenberg-Marquardt back propagation training function was used with a hyperbolic tangent sigmoid transfer function. There were 28 input nodes, one for each electrode pair in **S**, and 2 output nodes corresponding to the x and y coordinates. This results in a total of 157 neural network weights including bias weights. To avoid over-fitting, we should have 10 to 100 times more data points for training than the number of weights. The 100 randomly selected positions were each recorded 28 times for a total of 2800 data points. Both the data and x and y coordinates were normalised to [0,1]. The data was split into training, validation and testing data of 95%, 3% and 2% respectively. The validation set was randomly selected 10 times and a new model was trained for each. The model with the lowest mean squared error (MSE) was then selected.

The averaged mean squared error (MSE) for all ten models was 3.32mm^2 and the standard deviation was 1mm^2. The averaged Euclidean distance between the ground truth and predictions for all 11 randomly selected test positions was 2.03mm with a standard deviation of 0.26mm. Fig. 9 shows the error ellipses of the model with the lowest MSE and mean Euclidean distance which were 2.15mm^2 and 1.82mm respectively. The centre of each error ellipse was the mean of 6 predictions for a given ground truth position (A-K) while the span of the ellipse shows the standard deviation of the 6 predictions along the two principal component directions. If we consider a prediction to be correctly classified when the Euclidean distance is less than or equal to the probe radius of 2.75mm then 54 of the 66 predictions were correct (82%). When considering the error ellipse alone, 10 of the 11 mean values were considered correct (91%) with only the mean value for position B being incorrectly predicted. Point A lies on the edge of the convex hull that surrounds the data space yet is correctly predicted. The prediction for point B, which lies in the interior of the sensor, deviates from its ground truth but still remains close to the boundary of the probe. This error could potentially be due to the low sensitivity in that region. The quadrant area is thus a factor that needs to be determined depending on the intended use of the sensor. When trying to sense a more global change, such as soft body dynamics, large quadrants may be adequate. If more local changes are to be detected, such as the probe in this work, then the quadrant area may need to be reduced. Though ΔR_{eq} was greatest around the periphery, the neural network

correctly predicts points in the interior except point B.

V. CONCLUSION

This paper presents NeatSkin, a new soft robotic sensor skin employing discrete impedance tomography. NeatSkin employs a coarse channel network and is capable of sensing external stimuli with a relatively low output dimensionality and a high degree of accuracy. Consisting of liquid channels in a silicone skin, the sensory network does not significantly affect the mechanical properties of the base silicone material. NeatSkin could be easily added to existing robotic components as it is low cost and easy to fabricate. It is also readily simulated in order to determine the number of electrodes and network layout, including the maximum quadrant area, that is needed for a specific application. Future work will involve developing the NeatSkin approach into a 3D structure with a more complex network of channels, and ultimately using it to fabricate a soft robotic body. Channels with varying cross section and combining fluids of different resistivity are other extensions being considered. The signal generating and sensing circuits will be miniaturised using existing off the shelf electronic components in future iterations of the sensor.

VI. ACKNOWLEDGEMENTS

This work was partially supported by the EPSRC Centre for Doctoral Training in Future Autonomous and Robotic Systems (FARSCOPE) at the Bristol Robotics Laboratory. Hauser was supported by Leverhulme Trust RPG-2016-345. Rossiter was supported by EPSRC grants EP/M020460/1 and EP/M026388/1 and by the Royal Academy of Engineering as a Chair in Emerging Technologies.

REFERENCES

[1] B. Trimmer, "Soft robots and size," *Soft Robotics*, vol. 2, no. 2, pp. 49–50, 2015.

[2] E. Judd, G. Soter, J. Rossiter, and H. Hauser, "Sensing through the body-non-contact object localisation using morphological computation," in *2019 2nd IEEE International Conference on Soft Robotics (RoboSoft)*. IEEE, 2019, pp. 558–563.

[3] G. Soter, A. Conn, H. Hauser, and J. Rossiter, "Bodily aware soft robots: integration of proprioceptive and exteroceptive sensors," in *2018 IEEE International Conference on Robotics and Automation (ICRA)*. IEEE, 2018, pp. 2448–2453.

[4] K. M. Digumarti, A. T. Conn, and J. Rossiter, "Eumobot: replicating euglenoid movement in a soft robot," *Journal of the Royal Society Interface*, vol. 15, no. 148, p. 20180301, 2018.

[5] H. Hauser, K. Nakajima, and R. Füchslin, "Morphological computation–the body as a computational resource," *E-book on Opinions and Outlooks on Morphological Computation*, pp. 226–244, 2014.

[6] V. J. Lumelsky, M. S. Shur, and S. Wagner, "Sensitive skin," *IEEE Sensors Journal*, vol. 1, no. 1, pp. 41–51, 2001.

[7] S. Li, H. Zhao, and R. F. Shepherd, "Flexible and stretchable sensors for fluidic elastomer actuated soft robots," *MRS Bulletin*, vol. 42, no. 2, pp. 138–142, 2017.

[8] J. C. Yeo, C. T. Lim *et al.*, "Emerging flexible and wearable physical sensing platforms for healthcare and biomedical applications," *Microsystems & Nanoengineering*, vol. 2, p. 16043, 2016.

[9] A. S. Nittala, A. Withana, N. Pourjafarian, and J. Steimle, "Multi-touch skin: A thin and flexible multi-touch sensor for on-skin input," in *Proceedings of the 2018 CHI Conference on Human Factors in Computing Systems*. ACM, 2018, p. 33.

[10] O. Glauser, D. Panozzo, O. Hilliges, and O. Sorkine-Hornung, "Deformation capture via soft and stretchable sensor arrays," *ACM Transactions on Graphics (TOG)*, vol. 38, no. 2, p. 16, 2019.

[11] M. Teyssier, G. Bailly, C. Pelachaud, E. Lecolinet, A. Conn, and A. Roudaut, "Skin-on interfaces: A bio-driven approach for artificial skin design to cover interactive devices," in *The 32st Annual ACM Symposium on User Interface Software and Technology. ACM*.

[12] C. Larson, J. Spjut, R. Knepper, and R. Shepherd, "A deformable interface for human touch recognition using stretchable carbon nanotube dielectric elastomer sensors and deep neural networks," *Soft Robotics*, 2019.

[13] B. H. Brown, "Electrical impedance tomography (eit): a review," *Journal of Medical Engineering & Technology*, vol. 27, no. 3, pp. 97–108, 2003.

[14] Y. Kato, T. Mukai, T. Hayakawa, and T. Shibata, "Tactile sensor without wire and sensing element in the tactile region based on eit method," in *SENSORS, 2007 IEEE*. IEEE, 2007, pp. 792–795.

[15] A. Nagakubo, H. Alirezaei, and Y. Kuniyoshi, "A deformable and deformation sensitive tactile distribution sensor," in *2007 IEEE International Conference on Robotics and Biomimetics (ROBIO)*. IEEE, 2007, pp. 1301–1308.

[16] H. Alirezaei, A. Nagakubo, and Y. Kuniyoshi, "A tactile distribution sensor which enables stable measurement under high and dynamic stretch," in *2009 IEEE Symposium on 3D User Interfaces*. IEEE, 2009, pp. 87–93.

[17] H. Lee, D. Kwon, H. Cho, I. Park, and J. Kim, "Soft nanocomposite based multi-point, multi-directional strain mapping sensor using anisotropic electrical impedance tomography," *Scientific Reports*, vol. 7, no. 1, pp. 1–10, 2017.

[18] J.-B. Chossat, H.-S. Shin, Y.-L. Park, and V. Duchaine, "Soft tactile skin using an embedded ionic liquid and tomographic imaging," *Journal of Mechanisms and Robotics*, vol. 7, no. 2, 2015.

[19] T. Helps and J. Rossiter, "Proprioceptive flexible fluidic actuators using conductive working fluids," *Soft Robotics*, vol. 5, no. 2, pp. 175–189, 2018.

[20] Y.-N. Cheung, Y. Zhu, C.-H. Cheng, C. Chao, and W. W.-F. Leung, "A novel fluidic strain sensor for large strain measurement," *Sensors and actuators a: Physical*, vol. 147, no. 2, pp. 401–408, 2008.

[21] S. Han, T. Kim, D. Kim, Y.-L. Park, and S. Jo, "Use of deep learning for characterization of microfluidic soft sensors," *IEEE Robotics and Automation Letters*, vol. 3, no. 2, pp. 873–880, 2018.

[22] Y.-L. Park, B.-R. Chen, and R. J. Wood, "Design and fabrication of soft artificial skin using embedded microchannels and liquid conductors," *IEEE Sensors Journal*, vol. 12, no. 8, pp. 2711–2718, 2012.

[23] G. V. et al., "Ahkab: Open source electronic circuit simulation in python," https://ahkab.github.io/ahkab/, 2015.

[24] M. Garrad, G. Soter, A. Conn, H. Hauser, and J. Rossiter, "A soft matter computer for soft robots," *Science Robotics*, vol. 4, no. 33, 2019.

[25] N. J. Guliyev and V. E. Ismailov, "A single hidden layer feedforward network with only one neuron in the hidden layer can approximate any univariate function," *Neural Computation*, vol. 28, no. 7, pp. 1289–1304, 2016.